



1 **Technical Note: Noble gas extraction procedure and performance of the**
2 **Cologne Helix MC Plus multi-collector noble gas mass spectrometer for**
3 **cosmogenic neon isotope analysis**

4 Benedikt Ritter^{1*}, Andreas Vogt¹, Tibor J. Dunai^{1*}

5 ¹ University of Cologne, Institute of Geology and Mineralogy, Zùlpicher StraÙe 49b, Kùln 50674,
6 Germany

7 *Corresponding authors

8 Benedikt Ritter – benedikt.ritter@uni-koeln.de

9 Tibor J. Dunai – tdunai@uni-koeln.de

10 Keywords: Noble Gas, Mass Spectrometry, Cosmogenic Nuclides

11

12 **Abstract:**

13 We established a new laboratory for noble gas mass spectrometry that is dedicated for the
14 development and application to cosmogenic nuclides at the University of Cologne (Germany). At
15 the core of the laboratory are a state-of-the-art high mass resolution multicollector Helix MCPlus
16 (Thermo-Fisher) noble gas mass spectrometer and a novel custom-designed automated
17 extraction line. The Mass-spectrometer is equipped with five combined Faraday Multiplier
18 collectors, with $10^{12} \Omega$ and $10^{13} \Omega$ pre-amplifiers for faraday collectors. We describe the extraction
19 line and the automatized operation procedure for cosmogenic neon and the current performance of
20 the experimental setup. Performance tests were conducted using gas of atmospheric isotopic
21 composition (our primary standard gas); as well as CREU-1 intercomparison material, containing
22 a mixture of neon of atmospheric and cosmogenic composition. We use the results from repeated
23 analysis of CREU-1 to assess the performance of the current experimental setup at Cologne. The
24 precision in determining the abundance of cosmogenic ^{21}Ne is equal or better than those reported
25 for other laboratories. The absolute value we obtain for the concentration of cosmogenic ^{21}Ne in
26 CREU is indistinguishable from the published value.

27 **1. Introduction**

28 Cosmogenic Ne isotopes are stable and compared to other cosmogenic radionuclides (e.g. ^{10}Be ,
29 ^{26}Al) exhibit the potential to date beyond the physical limit of radionuclides. The particular
30 strength of cosmogenic neon is its application to date quartz clasts of very old surfaces ($>4\text{Ma}$) or
31 very slowly eroding landscapes ($<10\text{cm/Ma}$), which is unattainable with most other radionuclides
32 (Dunai, 2010). Cosmogenic Ne analysis can be applied to a range of neon-retentive minerals (e.g.,
33 quartz, olivine and pyroxene); amongst which quartz is the most commonly used. Ne can be
34 measured on conventional sector field noble gas mass spectrometers; is less time consuming and
35 requires less sample-preparation compared to AMS measurements required for the cosmogenic



36 radionuclides. Recent studies used cosmogenic Ne isotope geochronology for dating old surfaces
37 (e.g. Ritter et al., 2018; Dunai et al., 2005; Binnie et al., 2020), reconstructing erosion rates (e.g.
38 Ma et al., 2016), or applying $^{10}\text{Be}/^{21}\text{Ne}$ burial dating (e.g. McPhillips et al., 2016). The advantage
39 to use also other minerals than quartz, led to several studies using ^{21}Ne to date for example basalt
40 flows (e.g. Espanon et al., 2014; Gillen et al., 2010). Neon has three stable isotopes ^{20}Ne , ^{21}Ne , and
41 ^{22}Ne , of which ^{20}Ne is the most abundant; the atmospheric $^{21}\text{Ne}/^{20}\text{Ne}$ and $^{22}\text{Ne}/^{20}\text{Ne}$ ratios are
42 0.002959 ± 0.000022 and 0.1020 ± 0.0008 , respectively (Eberhardt et al., 1965). There are several
43 recent re-determinations of the atmospheric $^{21}\text{Ne}/^{20}\text{Ne}$ ratio (e.g. Honda et al., 2015; Wielandt and
44 Storey, 2019) one of which yields a $\sim 2\%$ lower value (Honda et al., 2015). For our evaluation of
45 our data, we utilize the $^{21}\text{Ne}/^{20}\text{Ne}$ value of Wielandt and Storey (2019) of 0.0029577 ± 0.0000014
46 and for $^{22}\text{Ne}/^{20}\text{Ne}$ that of Eberhardt et al. (1965). Note, that in the context of the determination of
47 the *abundance* of cosmogenic nuclides in a sample eventual differences between the used and the
48 actual value of the atmospheric $^{21}\text{Ne}/^{20}\text{Ne}$ ratio are unimportant, if (i) atmospheric neon is used
49 as calibration gas, (ii) the same value for the atmospheric composition of atmospheric neon is
50 used consistently throughout the evaluation of the isotope data (mass discrimination etc.) and
51 calculation of abundances and (iii) the atmospheric value used is reported along with the data.

52 All three neon isotopes are produced in about equal proportions by neutron spallation in quartz
53 (Niedermann et al., 1994). Due to the lower abundances of ^{21}Ne and ^{22}Ne as compared to ^{20}Ne in
54 air, and the ubiquitous presence of atmospheric neon in samples, any contribution from
55 cosmogenic production in samples is most easily picked up with the former two isotopes.
56 Consequently, the neon three-isotope diagram with ^{20}Ne as common denominator (Niedermann
57 et al., 1994; Niedermann, 2002) is customarily used to assess ^{21}Ne -data for the presence of
58 terrestrial cosmogenic Ne and its discrimination from other non-atmospheric Ne-components
59 (Dunai, 2010). The latter may be nucleonic Ne and/or mantle-derived Ne. Hence, the accurate
60 determination of cosmogenic Ne and its discrimination from other components requires the
61 accurate discrimination from any other component.

62 Common isobaric interferences for neon measurements are at $m/e = 20$ $^{40}\text{Ar}^{2+}$, H^{19}F^+ and $\text{H}_2^{18}\text{O}^+$
63 interfering with $^{20}\text{Ne}^+$, and at $m/e = 21$ $^{20}\text{NeH}^+$, interfering with $^{21}\text{Ne}^+$, and $^{44}\text{CO}_2^{2+}$ at $m/e = 22$
64 interfering with $^{22}\text{Ne}^+$. $^{40}\text{Ar}^{2+}$ and $^{12}\text{C}^{16}\text{O}_2^{2+}$ interferences are considered to be the main challenges
65 for neon analysis. Recent studies demonstrated the ability of the Helix MCPlus to fully resolve the
66 $^{40}\text{Ar}^{2+}$, H^{19}F^+ and $\text{H}_2^{18}\text{O}^+$ peaks from the $^{20}\text{Ne}^+$ peak (e.g. Honda et al., 2015; Wielandt and Storey,
67 2019) and its ability to reliably measure ^{21}Ne at an off-centre peak position that is free of
68 interference from $^{20}\text{NeH}^+$ (Honda et al., 2015; Wielandt and Storey, 2019). The remaining
69 interference of $^{12}\text{C}^{16}\text{O}_2^{2+}$ at $m/e = 22$ can be corrected via monitoring of the double/single-charged
70 ratio of CO_2 in-between samples (Honda et al., 2015) or the measurement of $^{13}\text{C}^{16}\text{O}_2^{2+}$ at $m/e =$
71 22.5 during sample analysis (Wielandt and Storey, 2019). Recently mass spectrometers with



72 higher resolution have become available, which permit almost full separation of $^{12}\text{C}^{16}\text{O}_2^{2+}$ and ^{22}Ne
73 (Farley et al., 2020).

74 Beside the resolution and characteristics of a noble gas mass spectrometer to resolve and
75 quantitatively determine neon compositions of an unknown sample, the calibration, sample
76 extraction and purification are crucial achieving accurate and reproducible results. Automation of
77 extraction protocols and workflows may assist in achieving a high degree of reproducibility by
78 eliminating inaccuracies or errors by operators having a variable degree of expertise. In this
79 paper, we describe the current setup of the noble gas mass spectrometer and its automated
80 extraction line that is located in the Institute of Geology and Mineralogy at the University of
81 Cologne (Germany), and we review its performance for neon analysis.

82 **2. Experimental setup**

83 **2.1 Noble gas mass-spectrometer**

84 The Cologne noble gas laboratory is equipped with a Helix MCPlus from Thermo Fisher Scientific
85 with five CFMs modules (Combined Faraday Multiplier), called 'Aura'. The mass spectrometer
86 configuration and performance is mostly equivalent to those described elsewhere (Honda et al.,
87 2015; Wielandt and Storey, 2019); here we describe potential differences in configuration and
88 performance parameters that may be unique to a given instrument.

89 In the instrument at Cologne University, all but one Faraday amplifier, are equipped with $10^{13} \Omega$
90 resistors, one with $10^{12} \Omega$ (H2). The L1 module has 0.3 mm wide collector slits, all other modules
91 have 0.6 mm wide slits. The CFM at L1 configuration is flipped (i.e., the relative positions of the
92 Faraday and Multiplier are swapped) as compared to the standard configuration, which is the only
93 difference from the standard configuration. The two SAES NP10 getters, at the source and the
94 multiplier block, are kept at room temperature during analysis.

95 For neon isotope analysis of calibrations and samples, we utilize the H1, Ax and L1 CFMs ($^{20}\text{Ne}^+$
96 L1 Faraday; $^{22}\text{Ne}^+$ H1 Faraday; $^{21}\text{Ne}^+$ L1 multiplier; CO_2^+ H1 Faraday; for blanks we utilize the L1
97 multiplier also for $^{20}\text{Ne}^+$ and $^{22}\text{Ne}^{++}$). With the widest source slit (0.25 mm) mass resolution (at 5%
98 peak valley) and mass resolving power (between 10% and 90% of peak) on the L1 detector with
99 0.3 mm collector slit width are approximately 1700 and 6500, respectively. For the Ax and H1
100 detectors with 0.6 mm collector slit, the corresponding values are approximately 1000 and 6000,
101 respectively. As such the system allows the interference-free determination of ^{20}Ne and ^{21}Ne ; for
102 ^{21}Ne this entails measuring at an off-centre peak position (Honda et al., 2015; Wielandt and Storey,
103 2019).



104 2.2 Extraction line

105 The original noble gas extraction and purification line has a modular design. Modules are (i)
106 extraction (currently only laser extraction; to be joined by a crushing device), (ii) calibration gas
107 pipettes and volumes, (iii) clean-up, and (iv) cryogenic separation. The calibration module is
108 physically linked to the clean-up module, the other modules can be separated, if required. Among
109 the common features of all modules is that, all valves and tubing in contact with the sample gas
110 are of metal; tubing is of stainless steel or vacuum-annealed copper. Furthermore, all valves used
111 for handling of sample and calibration gas are pneumatically actuated all-metal diaphragm valves
112 (Fujikin MEGA-M LA; FWB(R)-71-6.35), that can be operated at high temperature (up to 350°C).
113 Tubing and valves in contact with sample gas are continuously kept at constant temperature
114 between 160°C and 200°C; exceptions are the functional traps and portions of the tubing in the
115 cryogenic separation. Temperature is maintained with heating tapes (Horst HS 450°C) and is
116 controlled section-wise (Horst HT30). The temperature of the heated sections is controlled to
117 ±1°C. Thermal insulation is achieved with high-temperature resistant silicone foam (HOKOSIL®;
118 resists ≤280°C; permitting bake-out at higher than operation temperatures). Vacuum connections
119 used are VCR (for Fujikin Valves), CF (for adapters, getters and manifold in clean up) and Swagelok
120 (for flexible tubing between modules and between ports of the cryogenic separator (Swagelok 321
121 Stainless Steel Flexible Tubing with XBA adapter; and copper tubing). Tubing and valves are 1/4"
122 outer diameter (Swagelok) or equivalent (VCR, Fujikin). The overall internal volume of the
123 extraction line (laser-extraction, clean-up & cryogenic separation) is 530 cm³. Outside the volume
124 used for sample preparation, CF connections are used throughout. A schematic overview and
125 picture of the extraction line is provided in Fig. 1.

126 More specifically about the individual modules:

127 i. Laser extraction module: Energy for the heat-extraction is provided by an output-tuneable
128 600 W fiberlaser (Rofin StarFiber600) at 1064nm wavelength through galvanometer scanner
129 optics (Rofin RS S 14 163/67 0°) and a sapphire viewport (Kurt Lesker, VPZL-275DUS). Quartz
130 samples for neon-extraction are heated in 15 mm outer diameter tungsten cups with lids. For
131 neon-extraction of quartz, the heating occurs via scanning of the lids (scanning speed 20 cm/s;
132 rastering a circular area of 10 mm diameter) with a defocussed (~ 0.5 mm diameter) continuous
133 wave beam with 100W power for 15 min. Copper (melting point 1085°C), placed in the cup-
134 assemblies, melts at 80W laser power (15 min extraction time); we assume that at 100W laser
135 power the internal temperature is ≥1200°C. The temperature of the top of the tungsten lids is
136 monitored with a pyrometer (CellaTemp PA 29 AF 2/L; Keller HCW). The tungsten cups can hold
137 up to ~600 mg quartz, which is fully extracted at aforementioned conditions. The tungsten cups
138 are reused. When analysing quartz, tungsten cups are emptied with a suction micropicker
139 (Micropicker MPC100; VU Amsterdam), while remaining in the sample revolver. In cases where



140 samples are melted during extraction, tungsten cups could be cleaned in HF (then of course
141 outside the revolver). Up to eighteen tungsten cups are loaded in a sample revolver, housed in a
142 DN 200 CF flange-sandwich. The sample revolver is machined from molybdenum, which permits
143 the heating of the tungsten cups while being situated in the revolver. To minimize heat-loss
144 through conduction, the cups sit on shards of zirconia (synthetic, cubic-stabilized ZrO₂). For
145 sample loading the volume containing the revolver is vented and continuously flushed with high-
146 purity nitrogen. During laser extraction the pressure is monitored (MEAS EPB-C1 sensor, welded
147 into a male VCR connector; Disynet), in case of an eventual failure of the viewport, the extraction
148 volume is automatically purged with Ar. The laser extraction has a dedicated pumping unit
149 (Pfeiffer HiCube80); pressures attained after sample loading and heating of the revolver (via
150 short-term laser-heating – stepwise increased to 200W -of an empty tungsten cup; the external
151 housing flanges reach ~50°C during this treatment; temperatures in adjacent cups in the revolver
152 stay below 156,6°C, which was verified with Indium wire) are usually 5×10^{-9} mbar (the lower
153 limit of the pressure gauge used) after one night of pumping. Typical blanks, obtained via heating
154 of an empty tungsten cup assembly, are ~0.3 fmol Neon. A detailed description of this novel
155 laser-furnace will be provided elsewhere.

156 ii. Calibration gas pipette module: The gas-pipettes are assemblies of male and female
157 versions of pneumatically actuated Fujikin diaphragm valves (MEGA-M LA; FWB(R)-71-6.35); the
158 reservoirs were manufactured by Caburn-MDC, the insides of the reservoirs are electropolished.
159 We currently have three different gases available for noble gas calibration ('Linde', 'Air', 'RedAir').
160 'Linde' is a noble gas mixture in nitrogen (9.889±0.009% He, 10.00±0.01% Ne, 10.01±0.01% Ar,
161 0.00987±0.0003% Kr; 0.01023±0.00002% Xe; all uncertainties are ±2σ; remainder N₂; prepared
162 gravimetrically by Linde) the He is enriched in ³He (12.3±0.3 R_a; ±2σ), the remaining noble gases
163 have atmospheric composition. 'Air' is a reservoir of air at atmospheric pressure and 'RedAir' a
164 reservoir of air at reduced pressure. For the neon determinations we utilize 'RedAir'. The volumes
165 of all reservoirs and the pipettes have been determined using a gravimetrically calibrated gas
166 volume (an assembly of a Swagelok SS-4H valve and a Swagelok SS-4CS-TW-50 miniature
167 cylinder; repeatedly weighed (Satorius MSA524P-1000-DI) under vacuum and filled with air at a
168 temperature, pressure and relative humidity measured with traceable and/or certified sensors
169 (thermometer: testo 110; manometer: Greisinger GMH 3181-12, DKD certificate D19853, D-K-
170 15070-01-01; hygrometer: VWR traceable 628-0031) and pressure readings (MKS Baratron, Type
171 628FU5TCF1B) from repeated step-wise expansion of gasses into the pipette-reservoir
172 assemblies). The temperature in the room where these calibrations were conducted was stable to
173 ±0.5°C over the course of the calibrations. The volumes of the reservoir and pipette of 'RedAir' are
174 8740±35 cm³ and 1.4565±0.0006 cm³, respectively. For filling of the 'RedAir' reservoir one pipette
175 volume of air was expanded into the reservoir; the temperature, pressure and humidity at the



176 time of filling of the pipette were measured with a traceable and certified sensor (same as above).
177 The first pipette volume extracted from the 'RedAir' reservoir contained $4.0196 \pm 0.0027 \times 10^{-9} \text{ cm}^3$
178 atmospheric neon at standard temperature and pressure (179 ± 1 fmol atmospheric neon).

179 iii. Clean-up module ('Sputnik'): Arranged around a central hexagonal 8-port manifold
180 (Kimball Physics, 2.75" spherical hexagon) are the sample/calibration inlet, the pumping outlet, a
181 pipette leading to a residual gas analyser (Hiden HAL/3F PIC), two SAES NP50 getters (one
182 operated hot, the other at room temperature; getters are housed in SAES GP 50 W2F bodies; water
183 cooling is optional, not used during sample analysis), an optional expansion volume, an internally
184 heated capacitance manometer (MKS Baratron, Type 628FU5TCF1B; @ 100°C) and the outlet to
185 the cryogenic separation unit (Fig. 1). The sample/calibration inlet tubing has an auxiliary port,
186 which e.g., is used for the crushing extraction module (build around a T4S crushing unit, VU
187 Amsterdam). The clean-up module is pumped via a manifold connected through gate-valves (MDC
188 E-GV-1500M-P) to a turbopump (Pfeiffer HiPace 300; backed by a membrane pump, Pfeiffer MVP
189 030-3) and an iongetter pump (Agilent, Vacion 40 plus Starcell).

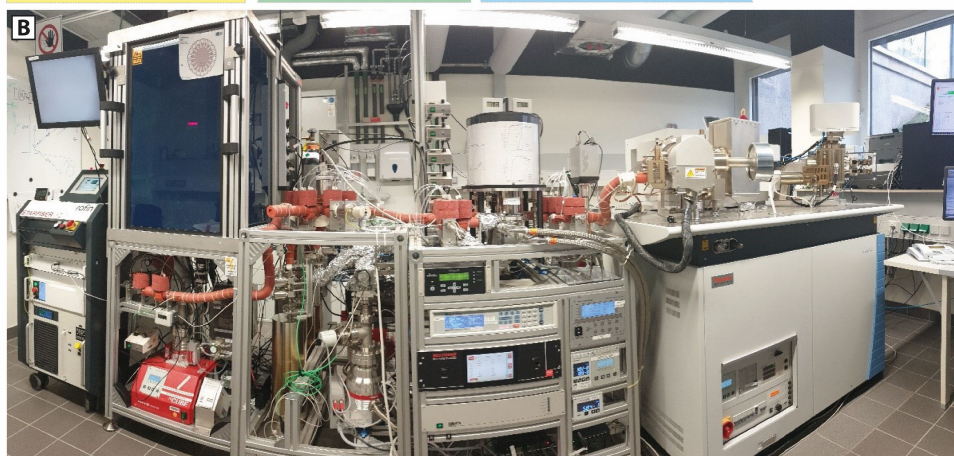
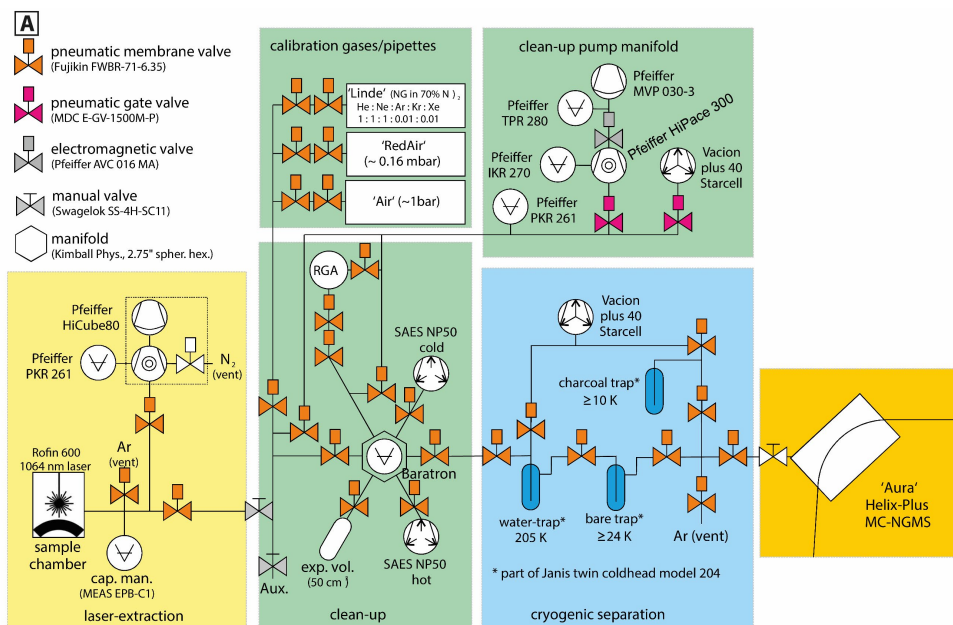
190 iv. Cryogenic separation module: Centre of this module is a double-cold trap unit (Janis, twin
191 coldhead model 204) that has inlet and outlet lines to three traps: a watertrap (operated at 205K)
192 a bare steel trap ($\geq 24\text{K}$) and a charcoal trap ($\geq 10\text{K}$). The cold trap unit is controlled by a
193 Lakeshore 336 Controller (Cryotronics). This module is pumped by an ion pump (Agilent, Vacion
194 40 plus Starcell).

195 The performance of the bare cold trap unit for He, Ne, Ar-separation was calibrated using the
196 Residual Gas Analyser (Hiden HAL/3F PIC). Neon is quantitatively adsorbed on the bare trap at
197 24 K, in equilibrium about 60% of the helium is adsorbed at 24 K. We use this to separate helium
198 from neon. Helium is removed (distilled-off in disequilibrium) either to the ion-pump or the 10K
199 charcoal head, the latter if the He is to be retained for analysis. Neon is fully released from the bare
200 trap at 80K, at this temperature argon is quantitatively retained on the bare trap, permitting
201 quantitative separation of the two gases.

202 Besides its functionality to separate noble gases from each other the bare trap serves as coldtrap
203 during Ne-analysis (held at 80 K) and replaces a liquid nitrogen cooled trap, which would
204 otherwise customarily be used for this purpose. The latter may introduce intensity fluctuations
205 during analysis due to changing coolant level, which we avoid with our set up. The last
206 pneumatically actuated valve before the Helix-Plus MCMS serves as inlet valve, the manual valve
207 of the Helix-Plus MCMS is permanently open.



208



209

210 *Fig. 1: (A) Schematic plan and picture (B) of the noble gas extraction and purification line at the*
 211 *University of Cologne. From left to right: Rofin Starfiber 600, full-protection laser-cage (laser*
 212 *protection windows P1P10, Laservision) housing the laser extraction, clean up unit, cryogenic*
 213 *separation unit and the Helix Plus NG-MCMS 'Aura'. The laboratory is temperature-stabilized to*
 214 *±0.5°C. Further description is provided in the text.*

215 **2.3 Automation**

216 The extraction and purification line can either be operated manually, via a switchboard for the
 217 pneumatic valves and the components' original controllers, or automatically via LabView. Manual



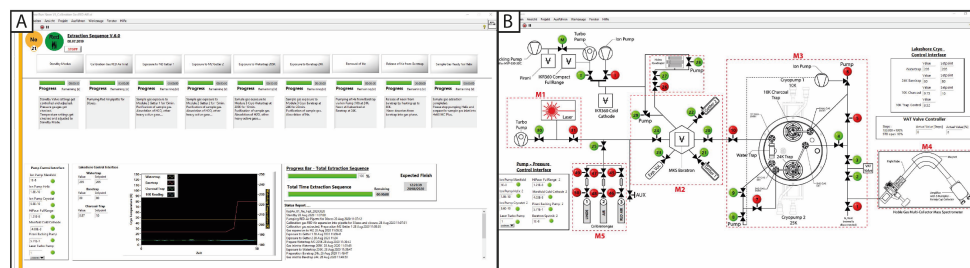
218 operation is mainly used for development of analytical routines, automatic operation generally
219 for sample and calibration-gas analysis. Automatic operation liberates the operator from
220 conducting necessarily repetitive tasks, thus helps to prevent mistakes and inconsistencies from
221 oversight or negligence; it allows to conduct gas purification and separation under precisely
222 identical conditions. The latter is also assisted by avoiding liquid coolants, which commonly are
223 affected by variable coolant levels (unless automatically filled with a suitably precise system or an
224 experienced and conscientious operator). Currently the laser system is operated manually (due
225 to safety regulations); all subsequent steps - until admission of the gas to the mass spectrometer
226 - are automated utilizing LabView (Version 2018) in a Windows 10 environment. The mass
227 spectrometry analysis of the purified gas is conducted with Qtegra (Thermo Fisher Scientific).

228 Valve control electronics were developed and implemented in-house, including digital
229 input/output modules (I/O modules from National Instruments) and RS-232 communication.
230 Main devices such as, SAES getter control, Lakeshore Cryo-Controller, turbo and ion-pumps
231 offered already LabView compatible Sub-VI's (Virtual Instrument), which were implemented into
232 the operation VI. The Agilent Ion Pump Control connection via the computer interfaces were
233 written/developed in-house.

234 The gauges and controllers of the Turbo pumps (Pfeiffer) and Ion pumps (Agilent) are monitored
235 via the operation VI. Automatic safety protocols are implemented to protect the extraction line
236 and equipment against sudden pressure increases. Temperature setting and monitoring of the
237 three cold traps (Janis Cryostat) is performed by the Lakeshore 336 controller, which in turn is
238 controlled via the operation VI.

239 LabView computing of the extraction sequence/protocol was programmed in single commands
240 and steps, joined into command sequences connected in series as sub-VIs for each extraction
241 protocol (various noble gases and sources of samples or calibration gas). Pressure and
242 temperature control sequences are programmed in continuous loop to ensure stability and safety
243 during operation. For handling, a structured user interface was designed (Fig. 2), which provides
244 the user with information about all parameters, total duration, and additionally logs every
245 extraction step.

246



247

248 *Fig. 2: Operating VIs of the Cologne Noble Gas Helix MCPlus. (A) The Neon VI informs the user in real*
249 *time about current data, such as pressure and temperature, as well as about the current status of the*
250 *preparation and the different extraction steps. The process is fully automatic, the user is informed*
251 *about the estimated extraction time. (B) Valve circuit overview.*

252 3. Analytical Procedure

253 Quartz samples are cleaned using standard procedures using dilute HF as etchant (Kohl and
254 Nishiizumi, 1992). Up to 600 mg of quartz are loaded into tungsten-cups and covered with a
255 tungsten-lid, the latter has a small opening in the lid to facilitate gas release. When opening the
256 laser furnace for re-loading, the furnace is vented and purged with a continuous flow of pure
257 nitrogen. In normal operation, after the initial installation and bake-out, the internal parts of the
258 furnace are never again exposed to air. The tungsten cups and lids remain in the nitrogen
259 atmosphere during sample (re-)loading. Cups are emptied with a suction micropicker
260 (Micropicker MPC100, VU Amsterdam) while seated in the revolver, and weighed samples are
261 transferred from glass vials through a miniature metal funnel (glass funnels produced undesirable
262 static effects) into the cups. After reloading, the sample revolver is heated by firing the laser on an
263 empty cup; pressure $<5 \times 10^{-9}$ mbar is usually achieved after pumping overnight. During this
264 clean-up, and during subsequent analyses, the temperature of adjacent cups does not exceed
265 156.6°C (verified with Indium wire). Cosmogenic Ne is extracted from quartz by heating the
266 sample with a defocussed laser beam at 100W for 15 min; at these settings the cup-insides reach
267 ~1200 °C. This temperature allows reliable extraction of cosmogenic neon (Vermeesch et al.,
268 2015). After heating the furnace, it is allowed to cool for five minutes before the sample is
269 expanded to the clean-up module.

270 For calibrations, the calibration gas is expanded for 30sec into the pipette, the pipette volume is
271 then expanded into the clean-up volume. After this step, purification is identical for sample and
272 calibration gases. The pipetting of calibration gas, and the purification of sample and calibration
273 gases, is fully automatized.

274 Reactive gases are removed by sequential exposure to two metal getters (SAES NP50); the first is
275 operated hot, the other at room temperature. The gas is exposed to each for 15 min. Subsequently



276 the gas is exposed to the water trap at 205K for 10min. The remaining inert gases are exposed to
277 the bare-metal trap at 24K for 20min, which is then pumped for 5 min to remove helium from the
278 sample gas. The trap is then isolated and heated to 80K, followed by five-minutes holding time for
279 re-equilibration. Neon is quantitatively released and argon is quantitatively retained on the trap.
280 Ensuing Ne gas is expanded into the Helix MCMS for analysis. The bare trap at 80 K remains
281 connected to the mass spectrometer during analysis, for pumping of CO₂ and Ar evolving from the
282 mass spectrometer.

283 The configuration of the Helix is described above. For maximum sensitivity and precision for
284 abundance determination (Wielandt and Storey, 2019), we use the widest (0.25 mm) source slit
285 for neon analysis. We run the source at an electron energy of 115 eV, trap current of 200 μA and
286 an acceleration voltage of 9.9 kV.

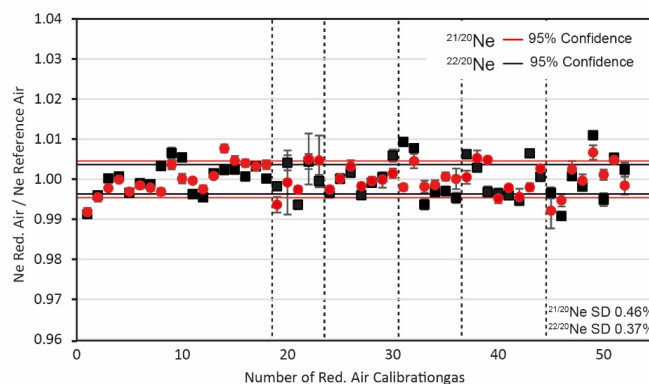
287 ²⁰Ne is measured on the high-resolution L1 Faraday cup (fitted with 10¹³ Ω pre-amplifier), fully
288 resolved from ⁴⁰Ar²⁺ and from molecular interferences such as HF⁺, H₂¹⁸O⁺. ²¹Ne is measured
289 off-centre on the high-resolution L1 multiplier, at a position that is free from interference from
290 ²⁰NeH⁺. ²²Ne is measured at peak centre on the H1 Faraday cup (fitted with 10¹³ Ω pre-amplifier);
291 interference from CO₂²⁺ is corrected via monitoring of the double/single-charged ratio of CO₂
292 in-between samples and measurement of CO₂ during sample analysis, which we found to be stable
293 at 0.0437±0.001 for our system throughout the period for which the data we report here were
294 obtained. The corresponding corrections of ²²Ne intensities are < 0.3% for one shot of ‘RedAir’
295 calibration gas (~17 fmol ²²Ne); the uncertainties of the correction are ~2 %, i.e., add < 0.006%
296 uncertainty of the intensity determinations for ‘RedAir’; these values scale linearly for smaller or
297 larger amounts of ²²Ne as found in samples. CO₂⁺ is measured on the Faraday cup of the Axial
298 collector (fitted with 10¹³ Ω pre-amplifier). We refrain from analysing the larger Neon-beams
299 (²²Ne, ²⁰Ne) on the multipliers, since we found that they are a significant source of CO₂ upon being
300 hit by beams larger than those typical for ²¹Ne signals (for analysing blanks, however, we use a
301 multiplier for ²⁰Ne and ²²Ne). Besides, the Faraday cups have a superior linearity and stability over
302 time (Wielandt and Storey, 2019). The mass spectrometer sensitivity, mass-discrimination and
303 multiplier vs. Faraday gain is calibrated with ‘RedAir’, which is measured at least once a day during
304 sample runs. Each batch of samples includes at least one measurement of ~100mg CREU-1
305 (Vermeesch et al., 2015) to monitor the performance of the extraction and purification system.
306 We are in the process of producing a new intercomparison material to replace CREU-1, whose
307 supplies are limited and eventually will run too low for regular use.

308 **4. Performance**

309 The within-run reproducibility of Neon-isotope ratios as determined for calibration gas (‘RedAir’,
310 ~ 17 fmol atmospheric Ne) is similar for ²¹Ne/²⁰Ne and ²²Ne/²⁰Ne ratios, with 0.46% and 0.37%

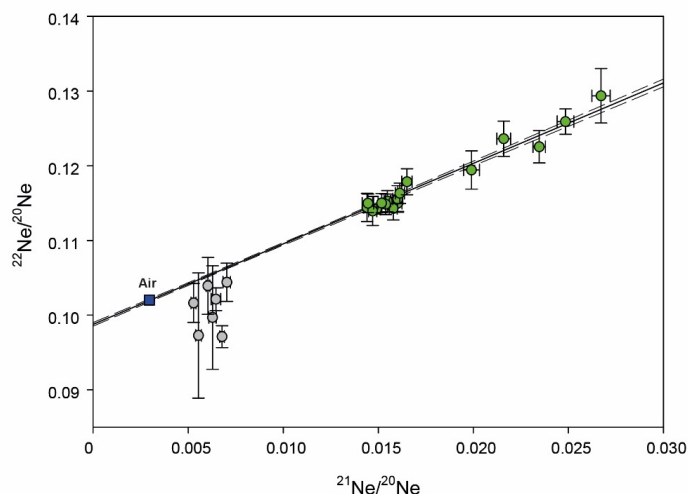


311 ($\pm 1\sigma$, $n=52$), respectively. This dispersion is larger than the uncertainty of individual
312 measurements (Fig. 3); this feature, and the values for dispersion, are similar to those reported
313 for other Helix Plus instruments (Honda et al., 2015; Wielandt and Storey, 2019). We use the
314 means and the uncertainty of the means of calibrations within runs to calibrate the measurements
315 samples, i.e., propagate the observed dispersion in calculations of the abundance of cosmogenic
316 ^{21}Ne in samples. The calculated cosmogenic ^{21}Ne abundances from 22 aliquots of CREU-1 (Table
317 1) all agree within 2σ with their arithmetic mean ($348 \pm 10 \times 10^6$ atoms/g; $\pm 2\sigma$); thus, we may
318 calculate an error-weighted mean: $348 \pm 2 \times 10^6$ atoms/g ($\pm 2\sigma$), which is indistinguishable from
319 the published value ($348 \pm 10 \times 10^6$ atoms/g; Vermeesch et al., 2015). We conclude that the
320 reproducibility and accuracy of the current set up at the University of Cologne for determining
321 cosmogenic ^{21}Ne in quartz is similar to or better than those reported for other laboratories
322 worldwide (Vermeesch et al., 2015; Farley et al., 2020; Ma et al., 2015).



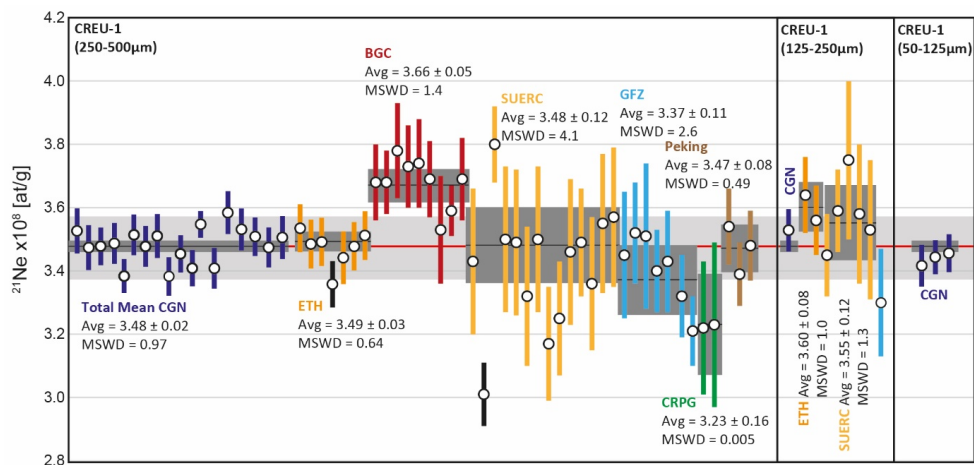
323

324 *Fig. 3: Reproducibility of standard gas 'RedAir' measurements for sample runs, during the period*
325 *between March 2020 and December 2020. Isotopic ratios are normalized to air for each run (mean*
326 *of isotope ratios obtained in run/atmospheric ratio). Stippled black lines delineate individual runs.*
327 *Error bars on individual data points are $\pm 1\sigma$.*



328

329 *Fig. 4: Neon-three-isotope plot for CREU-1 intercomparison material measured in Cologne. Error*
 330 *bars are $\pm 1 \sigma$. The cloud of green symbols are single-step CREU extractions (100W-15min), the green*
 331 *dots to the right of the cluster are the initial heating steps of stepwise extractions (at varying laser*
 332 *output), grey symbols are the subsequent steps that invariably had low abundance; for details see*
 333 *Table 1. Data of samples depicted in green are included in the regression calculation; data of the grey*
 334 *are excluded. The slope of the regression of the data (forced through air) is 1.078 ± 0.022 ($\pm 2\sigma$), which*
 335 *is indistinguishable from the published value of 1.108 ± 0.014 ($\pm 2\sigma$; Vermeesch et al., 2015). The*
 336 *dotted line denotes the 95% confidence interval.*



337

338 *Fig. 5: Compilation of measured CGN CREU-1 ^{21}Ne concentrations ($\pm 2\sigma$ uncertainties), compared to*
 339 *reported ^{21}Ne concentrations from interlaboratory comparison from Vermeesch et al. (2015) and*
 340 *recent data from the Peking noble gas lab from Ma et al. (2015). Black bars were considered outliers*



341 by the original authors and not used for calculation of averages (Vermeesch et al., 2015). The data is
 342 divided into three sections, each for a different CREU-1 grain-size analysed. The average ^{21}Ne
 343 concentration for CREU-1 of $3.48 \pm 10 \times 10^8$ at/g reported by Vermeesch et al. (2015) is marked as
 344 light-grey band and a red line for the mean. Lab-individual error-weighted means are displayed as
 345 black lines with their respective uncertainty in dark grey. The average obtained for CREU-1 at
 346 Cologne (all grain-sizes, $n=22$) is $3.48 \pm 0.02 \times 10^8$ at/g ($\pm 2 \sigma$; error-weighted standard deviation).
 347 The MSWD values (Mean Square of the Weighted Deviates ('reduced Chi-square', McIntyre et al.
 348 (1966)) are reported for all individual laboratory-means (Vermeesch et al., 2015; this study).

349 Table 1: CREU Data

Sample ID	Mass	Extraction	^{20}Ne		21/20		22/20		$^{21}\text{Ne}^*$	
	[g]	Power [W]	[10^9 at/g]						[10^6 at/g]	
01_CREU1 250-500 μm	0.0997	100	30.97	± 0.15	0.01434	± 0.00014	0.11381	± 0.00129	352.7	± 3.6
02_CREU1 250-500 μm	0.0993	100	29.81	± 0.24	0.01461	± 0.00015	0.11415	± 0.00129	347.4	± 3.5
03_CREU1 50-125 μm	0.1038	100	24.89	± 0.15	0.01669	± 0.00012	0.11646	± 0.00170	341.7	± 3.3
04_CREU1 50-125 μm	0.1319	100	25.73	± 0.20	0.01634	± 0.00018	0.11727	± 0.00089	344.4	± 2.7
05_CREU1 50-125 μm	0.1179	100	24.86	± 0.17	0.01686	± 0.00017	0.11614	± 0.00130	345.6	± 3.0
06_CREU1 125-250 μm	0.1078	100	27.00	± 0.35	0.01603	± 0.00022	0.11499	± 0.00110	352.9	± 3.3
07_CREU1 250-500 μm	0.1210	100	29.13	± 0.36	0.01490	± 0.00021	0.11417	± 0.00065	347.8	± 3.0
08_CREU1 250-500 μm	0.1105	100	30.46	± 0.25	0.01441	± 0.00018	0.11443	± 0.00189	348.7	± 3.2
09_CREU1 250-500 μm	0.1312	100	26.37	± 0.32	0.01579	± 0.00021	0.11428	± 0.00153	338.4	± 2.7
10_CREU1 250-500 μm	0.1128	100	29.92	± 0.40	0.01470	± 0.00022	0.11395	± 0.00195	351.4	± 3.2
11_CREU1 250-500 μm	0.1113	100	26.60	± 0.33	0.01603	± 0.00026	0.11556	± 0.00179	347.8	± 3.2
12_CREU1 250-500 μm	0.1053	100	30.56	± 0.36	0.01445	± 0.00030	0.11498	± 0.00125	351.1	± 3.5
13_CREU1 250-500 μm	0.1125	100	27.01	± 0.24	0.01548	± 0.00017	0.11526	± 0.00143	338.3	± 3.0
14_CREU1 250-500 μm	0.1210	100	26.21	± 0.30	0.01614	± 0.00024	0.11632	± 0.00137	345.4	± 3.0
15_CREU1 250-500 μm	0.1252	100	25.16	± 0.19	0.01651	± 0.00027	0.11786	± 0.00174	340.9	± 2.9
16_CREU1 250-500 μm	0.2063	100	28.54	± 0.33	0.01539	± 0.00020	0.11485	± 0.00137	354.8	± 2.1
17_CREU1 250-500 μm	0.1077	100	27.90	± 0.30	0.01518	± 0.00019	0.11502	± 0.00129	340.9	± 3.2
18_CREU1 250-500 μm	0.1126	30	16.44	± 0.16	0.02160	± 0.00036	0.12362	± 0.00236		
	0.1126	50	8.61	± 0.08	0.00628	± 0.00019	0.09968	± 0.00692		
	0.1126	70	5.71	± 0.05	0.00528	± 0.00013	0.10162	± 0.00260		
	0.1126	100	3.92	± 0.05	0.00554	± 0.00015	0.09727	± 0.00838	358.5	± 3.4
19_CREU1 250-500 μm	0.1111	24	11.96	± 0.17	0.02672	± 0.00048	0.12936	± 0.00364		
	0.1111	100	18.06	± 0.23	0.00678	± 0.00012	0.09711	± 0.00146	353.2	± 3.3
20_CREU1 250-500 μm	0.1301	24	14.27	± 0.12	0.02347	± 0.00033	0.12255	± 0.00217		



	0.1301	100	16.51 ± 0.18	0.00646 ± 0.00025	0.10213 ± 0.00152	350.9 ± 3.0
21_CREU1 250-500µm	0.1180	30	13.11 ± 0.15	0.02485 ± 0.00044	0.12592 ± 0.00170	
	0.1180	100	14.79 ± 0.09	0.00703 ± 0.00020	0.10440 ± 0.00256	347.5 ± 3.2
22_CREU1 250-500µm	0.1075	50	18.42 ± 0.12	0.01991 ± 0.00042	0.11944 ± 0.00256	
	0.1075	100	12.35 ± 0.11	0.00604 ± 0.00010	0.10391 ± 0.00381	350.6 ± 3.4

350

351 **Conclusion**

352 The performance of the set-up for Neon-isotope measurements in the new noble gas laboratory
353 at the University Cologne permits state-of-the art analysis of cosmogenic neon. We now regularly
354 perform analysis of samples for cosmogenic neon for our running projects; and are open to new
355 scientific cooperations.

356 **Author contribution:**

357 TJD, BR, AV build-up of the noble gas system. TJD, BR performance experiments and tests. BR, TJD
358 manuscript writing.

359 **Data Availability:**

360 The authors confirm that the data supporting the findings of this study are available within the
361 article.

362 **Acknowledgements:**

363 The equipment for the noble gas mass spectrometry laboratory described in this paper was
364 funded by Deutsche Forschungsgemeinschaft (DFG) - project number 259990027 to TJD. The
365 performance test was conducted and funded in the framework of the Collaborative Research
366 Center 1211 – Earth Evolution at the Dry Limit, Deutsche Forschungsgemeinschaft (DFG) - project
367 number 268236062 – SFB 1211. Special thanks go to Dave Wanless for patient training and
368 continuing support in mastering ‘Aura’.

369 **Declaration of interest**

370 The authors declare that the research was conducted in the absence of any commercial or financial
371 relationships that could be construed as a potential conflict of interest.

372 **References**

- 373 Binnie, S., Reicherter, K., Victor, P., González, G., Binnie, A., Niemann, K., Stuart, F., Lenting, C., Heinze,
374 S., Freeman, S., and Dunai, T. J.: The origins and implications of paleochannels in hyperarid, tectonically
375 active regions: The northern Atacama Desert, Chile, *Global and Planetary Change*, 185, 103083, 2020.
376
377 Dunai, T. J.: *Cosmogenic Nuclides: Principles, concepts and applications in the Earth surface sciences*,
378 Cambridge University Press 2010.



379

380 Dunai, T. J., Lopez, G. A. G., and Juez-Larre, J.: Oligocene-Miocene age of aridity in the Atacama Desert
381 revealed by exposure dating of erosion-sensitive landforms, *Geology*, 33, 321-324, 10.1130/g21184.1,
382 2005.

383

384 Eberhardt, P., Eugster, O., and Marti, K.: A redetermination of the isotopic composition of atmospheric
385 neon, *Zeitschrift für Naturforschung*, 20a, 623-624, 1965.

386

387 Espanon, V. R., Honda, M., and Chivas, A. R.: Cosmogenic ^3He and ^{21}Ne surface exposure dating of
388 young basalts from Southern Mendoza, Argentina, *Quaternary Geochronology*, 19, 76-86, 2014.

389

390 Farley, K., Treffkorn, J., and Hamilton, D.: Isobar-free neon isotope measurements of flux-fused
391 potential reference minerals on a Helix-MC-Plus10K mass spectrometer, *Chemical Geology*, 537,
392 119487, 2020.

393

394 Gillen, D., Honda, M., Chivas, A. R., Yatsevich, I., Patterson, D. B., and Carr, P. F.: Cosmogenic ^{21}Ne
395 exposure dating of young basaltic lava flows from the Newer Volcanic Province, western Victoria,
396 Australia, *Quaternary Geochronology*, 5, 1-9, 2010.

397

398 Honda, M., Zhang, X., Phillips, D., Hamilton, D., Deerberg, M., and Schwieters, J. B.: Redetermination
399 of the ^{21}Ne relative abundance of the atmosphere, using a high resolution, multi-collector noble gas
400 mass spectrometer (HELIX-MC Plus), *International Journal of Mass Spectrometry*, 387, 1-7, 2015.

401

402 Kohl, C. and Nishiizumi, K.: Chemical isolation of quartz for measurement of in-situ-produced
403 cosmogenic nuclides, *Geochimica et Cosmochimica Acta*, 56, 3583-3587, 1992.

404

405 Ma, Y., Wu, Y., Li, D., and Zheng, D.: Analytical procedure of neon measurements on GV 5400 noble
406 gas mass spectrometer and its evaluation by quartz standard CREU-1, *International Journal of Mass
407 Spectrometry*, 380, 26-33, 2015.

408

409 Ma, Y., Wu, Y., Li, D., Zheng, D., Zheng, W., Zhang, H., Pang, J., and Wang, Y.: Erosion rate in the
410 Shapotou area, northwestern China, constrained by in situ-produced cosmogenic ^{21}Ne in long-
411 exposed erosional surfaces, *Quaternary Geochronology*, 31, 3-11, 2016.

412

413 McIntyre, G., Brooks, C., Compston, W., and Turek, A.: The statistical assessment of Rb-Sr isochrons,
414 *Journal of Geophysical Research*, 71, 5459-5468, 1966.

415

416 McPhillips, D., Hoke, G. D., Liu-Zeng, J., Bierman, P. R., Rood, D. H., and Niedermann, S.: Dating the
417 incision of the Yangtze River gorge at the First Bend using three-nuclide burial ages, *Geophysical
418 Research Letters*, 43, 101-110, 2016.

419

420 Niedermann, S.: Cosmic-ray-produced noble gases in terrestrial rocks: dating tools for surface
421 processes, *Reviews in Mineralogy and Geochemistry*, 47, 731-784, 2002.

422



- 423 Niedermann, S., Graf, T., Kim, J., Kohl, C., Marti, K., and Nishiizumi, K.: Cosmic-ray-produced ^{21}Ne in
424 terrestrial quartz: the neon inventory of Sierra Nevada quartz separates, *Earth and Planetary Science*
425 *Letters*, 125, 341-355, 1994.
426
- 427 Ritter, B., Stuart, F. M., Binnie, S. A., Gerdes, A., Wennrich, V., and Dunai, T. J.: Neogene fluvial
428 landscape evolution in the hyperarid core of the Atacama Desert, *Scientific Reports*, 8, 13952,
429 10.1038/s41598-018-32339-9, 2018.
430
- 431 Vermeesch, P., Balco, G., Blard, P. H., Dunai, T. J., Kober, F., Niedermann, S., Shuster, D. L., Strasky, S.,
432 Stuart, F. M., Wieler, R., and Zimmermann, L.: Interlaboratory comparison of cosmogenic Ne-21 in
433 quartz, *Quaternary Geochronology*, 26, 20-28, 10.1016/j.quageo.2012.11.009, 2015.
434
- 435 Wielandt, D. and Storey, M.: A new high precision determination of the atmospheric ^{21}Ne abundance,
436 *Journal of Analytical Atomic Spectrometry*, 34, 535-549, 2019.
437